iScience

CellPress
OPEN ACCESS

Article

High-throughput single-cell antibody secretion quantification and enrichment using droplet microfluidics-based FRET assay

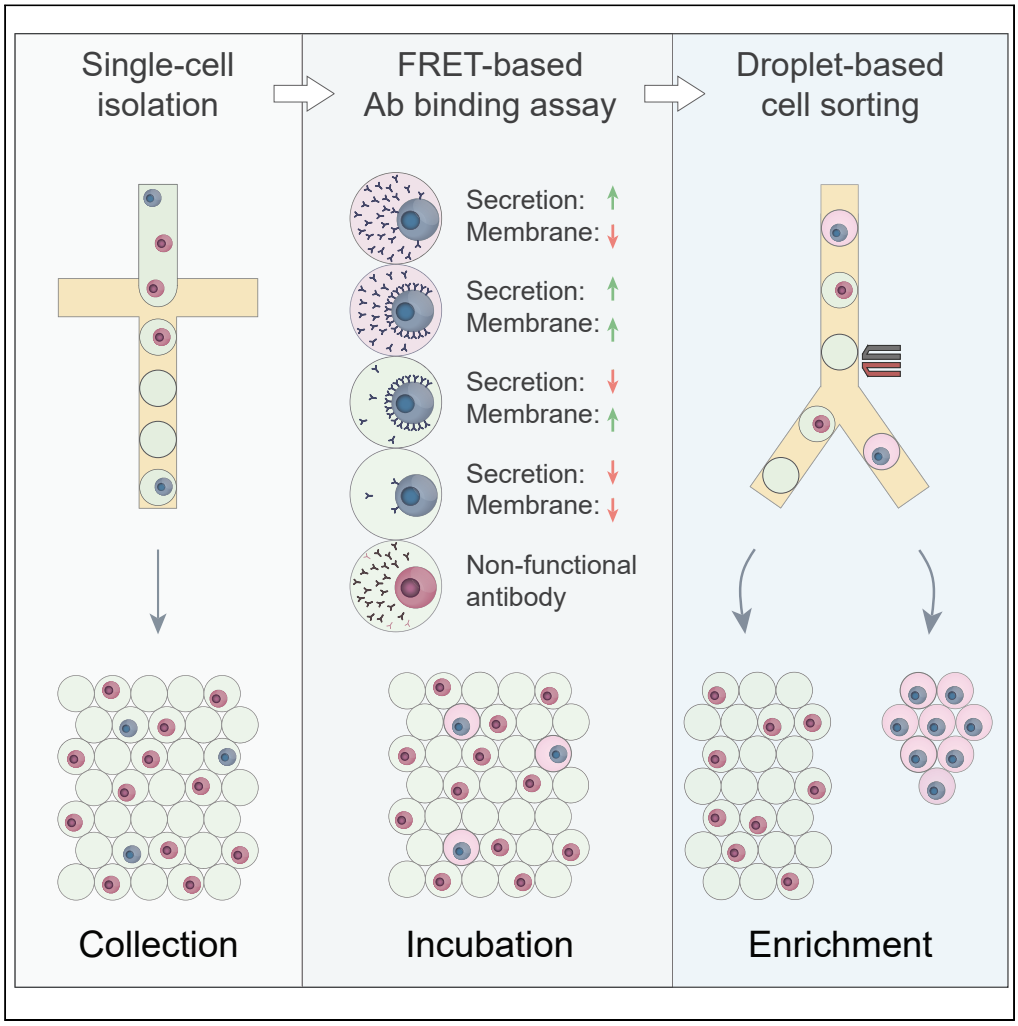

Justina Rutkauskaite, Simon Berger, Stavros Stavrakis, ..., Xavier Casadevall i Solvas, Andrew deMello, Linas Mazutis

andrew.demello@chem.ethz.ch (A.d.)
linas.mazutis@bti.vu.lt (L.M.)

Highlights

FRET-based screening assay of antibody-secreting cells in microfluidic droplets

Membrane-bound and secreted antibodies of the same cell are efficiently differentiated

Using mouse hybridoma cells antibody secretion assay is completed in 30 min

FRET-based droplet sorting enables over 800-fold enrichment in one round of sorting

Rutkauskaite et al., iScience *25*, 104515
July 15, 2022
https://doi.org/10.1016/j.isci.2022.104515

iScience

CellPress
OPEN ACCESS

Article

High-throughput single-cell antibody secretion quantification and enrichment using droplet microfluidics-based FRET assay

Justina Rutkauskaite,[1,2] Simon Berger,[2] Stavros Stavrakis,[2] Oliver Dressler,[2] John Heyman,[3] Xavier Casadevall i Solvas,[4] Andrew deMello,[2,*] and Linas Mazutis[1,5,*]

SUMMARY

High-throughput screening and enrichment of antibody-producing cells have many important applications. Herein, we present a droplet microfluidic approach for high-throughput screening and sorting of antibody-secreting cells using a Förster resonance electron transfer (FRET)-based assay. The FRET signal is mediated by the specific binding of the secreted antibody to two fluorescently labeled probes supplied within a droplet. Functional hybridoma cells expressing either membrane-bound or secreted monoclonal antibodies (mAbs), or both, were efficiently differentiated in less than 30 min. The antibody secretion rate by individual hybridoma cells was recorded in the range of 14,000 Abs/min, while the density of membrane-bound fraction was approximately 100 Abs/μm^2. Combining the FRET assay with droplet-based single-cell sorting, an 800-fold enrichment of antigen-specific cells was achieved after one round of sorting. The presented system overcomes several key limitations observed in conventional FACS-based screening methods and should be applicable to assaying various other secreted proteins.

INTRODUCTION

Since the first discovery of B-cells approximately 50 years ago by Max Cooper and Robert Good, monoclonal antibodies (mAbs) remain one of the most utilized biomolecules in cancer therapy ("biologics") and diagnostics (Chan and Chan, 2017; Cooper et al., 1965; Gitlin et al., 2015). Owing to their wide application in biomedicine, the market for mAbs has grown steadily from $39 billion in 2008 to $115.2 billion in 2018 (Lu et al., 2020). However, despite this growing demand, techniques for high-throughput discovery of monoclonal antibodies (mAbs) with novel specificities and properties have lagged behind, partly due to the limited sensitivity of antibody-binding assays, and partly due to technical difficulties associated with efficient isolation of positive, mAb-producing cells. Consequently, new technological solutions enabling the rapid identification of mAbs against a target of interest remain highly desirable.

Although individual cells expressing mAbs can be successfully isolated into 96- or 384-well microtiter plates using fluorescence-activated cell sorting (FACS), harvesting FACS-sorted cells *ex vivo* is problematic due to poor survival rates and typically low levels of secreted mAbs (Auner et al., 2010; Cocco et al., 2012; Nojima et al., 2011). As a result, mAb discovery often relies on the formation of hybridoma cells (i.e., fusion of IgG-expressing B cells with myeloma cells to generate an immortalized antibody-producing cell) followed by a limiting dilution step, to isolate and clonally expand individual antibody-secreting cells (ASCs) (Frenzel et al., 2017; Liu, 2014; Pasqualini and Arap, 2004). Screening of a few thousand cells in this fashion is feasible, however, at a cost of significant labor, extended screening times, and excessive reagent consumption (Seah et al., 2018). Significantly higher throughput can be achieved using antibody phage display (Smith, 1985) or ribosome display (Azizi et al., 2012) methods. Unfortunately, these approaches do not preserve the native heavy and light chain pairing, and fail to produce post-translational modifications necessary for antibody folding and/or activity (Chan et al., 2014; Drabek et al., 2016; Frenzel et al., 2013).

In recent years, microfluidic methods have emerged as a powerful alternative to the conventional mAb discovery techniques (Akbari and Pirbodaghi, 2014; Debs et al., 2012; Ding et al., 2020; Fitzgerald et al., 2015; Love et al., 2006; Mazutis et al., 2013; Singhal et al., 2010). Early examples of single-cell antibody assays,

[1]Institute of Biotechnology, Life Sciences Centre, Vilnius University, 7 Sauletekio ave., 10257 Vilnius, Lithuania

[2]Institute for Chemical and Bioengineering, ETH Zurich, Vladimir Prelog Weg 1, 8093 Zürich, Switzerland

[3]Harvard University, SEAS, 9 Oxford St., Cambridge, MA 02139, USA

[4]MeBioS division, Department of Biosystems, KU Leuven, Willem de Croylaan 42, 3001 Leuven, Belgium

[5]Lead contact

*Correspondence: andrew.demello@chem.ethz.ch (A.d.), linas.mazutis@bti.vu.lt (L.M.)

https://doi.org/10.1016/j.isci.2022.104515

with cells isolated using on-chip valves (Singhal et al., 2010), nano-wells (Love et al., 2006), or microcapillary arrays (Chen et al., 2016) demonstrated the high potential of microfluidic technologies. However, even when using these approaches, screening remains limited to between 10^3 and 10^4 cells, while recovery of positive clones remains a technological challenge. In the context of the human immune system, which is expected to comprise over 10^{11} B cells, significantly higher throughput methodologies, such as those based on droplet-based microfluidics, are required (Fischer, 2011). Here, millions of highly monodisperse droplets can be produced at high throughput (over 1000 droplets per second), where each droplet represents an independent reaction vessel, isolated by an immiscible carrier fluid. In addition, droplets can be precisely manipulated utilizing a whole host of unit operations, such as merging, splitting, and sorting (Guo et al., 2012; Mazutis et al., 2013; Rakszewska et al., 2014; Shembekar et al., 2016). Cells can therefore be efficiently isolated from one another, and cells of interest can be sorted and recovered at high throughput (Shembekar et al., 2016). Importantly, as all biomolecules produced by the encapsulated cells remain within the droplets, a direct linkage between the phenotype (e.g., protein-binding activity) and genotype (encoding DNA or RNA) can be established (Bounab et al., 2020; Guo et al., 2012; Mazutis et al., 2013; Rakszewska et al., 2014; Shembekar et al., 2016). Furthermore, because droplet volumes in microfluidic devices are more than 1000 times lower than the well volumes of microtiter plates, detectable molecule concentrations are reached within short periods of time (Dressler et al., 2014; Eyer et al., 2017; Mazutis et al., 2013; Rakszewska et al., 2014; Shembekar et al., 2016). This not only allows high-throughput sample processing but also greatly reduces reagent costs compared to conventional assays.

While droplet-based microfluidic methods have vastly accelerated biological research, as well as significantly reducing development cost, the detection of antibody-binding activity has remained a challenging task, with only a few notable approaches described to date (Akbari and Pirbodaghi, 2014; Bounab et al., 2020; Debs et al., 2012; Ding et al., 2020; Gérard et al., 2020; Mazutis et al., 2013). For example, *Debs* et al. reported an integrated droplet-based microfluidic system for cell screening and sorting based on a mAb's capability to inhibit the enzymatic activity of a co-encapsulated drug target (Debs et al., 2012). More recently, simplified sandwich-ELISA protocols in picoliter-volume droplets were implemented for single-cell isolation of mAbs based on antigen-binding activity (Ding et al., 2020) and for single-cell activity-based screening and sequencing (Gérard et al., 2020). Commercial platforms such as Cyto-Mine (Josephides et al., 2020) and Celli*GO*^{TM} (Gérard et al., 2020) are now offering integrated solutions for screening Ab-producing cells. However, despite these exciting developments, a high-throughput single-cell platform enabling simultaneous quantification of functional activities and production rates of both cell-surface and secreted proteins of individual cells has been lacking.

Herein, we present a droplet-based microfluidic approach for high-throughput screening of antibody-secreting single-cells using a Förster resonance electron transfer (FRET)-based detection assay. To showcase the applicability of this approach, we encapsulated a mixture of 7R2/A4 and 9E10 hybridoma cells in 40 pl volume droplets, along with a fluorescently labeled secondary antibody (detection antibody) and a fluorescently labeled antigen (c-myc peptide). Antibodies released by cells of interest interact with the co-encapsulated detection antibodies and antigens, forming a ternary structure. Presence of these complexes is detected through FRET between the two fluorescently labeled molecules upon excitation of the donor fluorophore (detection antibody). Importantly, the FRET reaction only occurs in the presence of the secreted antibody, since only then will the probe molecules (donor and acceptor) bind and be brought into proximal contact. Droplets are analyzed using a microfluidic droplet-based screening platform, and cells of interest sorted based on the intensity of the detected FRET signal. Because all components necessary for the FRET-based assay are distributed homogeneously throughout all droplets, all cells in a population can be analyzed, in contrast to bead-based assays that rely on rare, bead and cell co-encapsulation events. In addition to the high selectivity of the FRET process, the inherently low background fluorescence levels associated with the FRET reaction ensure high sensitivity, without the need for complex multi-step operations, or washing steps required in conventional protocols.

RESULTS

Development of the FRET-based antibody detection assay

For an antibody-secretion assay to be broadly applicable, it must fulfill two general criteria. First, it needs to ensure unbiased detection of every cell within a heterogeneous population. Second, it should be quantitative, highly specific, and compatible with high-throughput screening approaches. A binding assay based on FRET fulfills both the aforementioned requirements and enables identification of different types of cells;

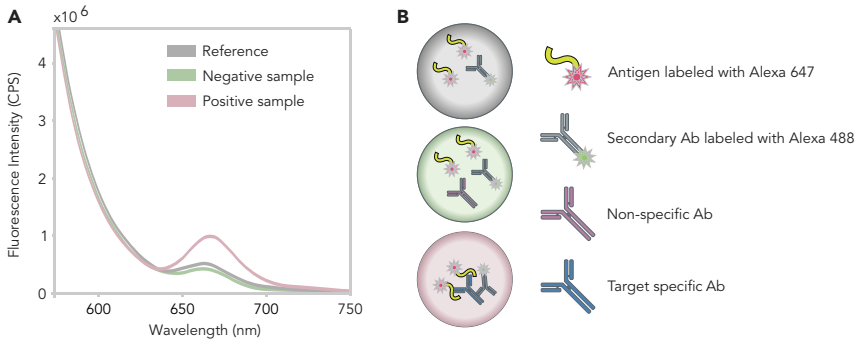

Figure 1. Evaluation of FRET-based antibody binding signals

(A) Comparison of the fluorescence emission spectra associated with positive, negative, and reference samples upon excitation at 488 nm. The positive sample comprises Alexa Fluor 488-labeled secondary antibody (FRET donor), Alexa Fluor 647-labeled c-myc peptide (FRET acceptor), and anti-c-myc antibody. These components form a ternary complex, bringing the donor and acceptor molecules into closeness, proximity. This results in FRET excitation of the Alexa Fluor 647 dye, and an emission peak at 668nm. The negative and reference samples contain the same FRET donor/acceptor pair and either a negative control primary antibody (directed against IFN-γ) or no primary antibody, respectively. These samples display no discernible emission of Alexa Fluor 647. Hence, the FRET reaction only occurs in the presence of the antigen-specific antibody. CPS – counts per second.

(B) Schematics of droplets containing different combinations of assay reagents.

(1) secretors—cells for which secreted antibodies constitute the majority of their Ab pool, (2) producers—cells for which membrane-associated antibodies constitute the main fraction of the entire Ab pool, and (3) non-producers—cells that do not produce antibodies in detectable quantities.

We selected two fluorophores, Alexa Fluor 488 and Alexa Fluor 647 as the FRET donor/acceptor pair, conjugated to an anti-mouse F(ab')2-specific polyclonal antibody and a c-myc peptide, respectively. In the presence of the antigen-specific mAb, both the anti-mouse F(ab')2 antibody and the c-myc peptide bind to the secreted antibody forming a ternary structure, with both fluorophores being within the Förster distance (<10 nm) of each other. In the presence of non-specific antibodies, the detection antibodies remain free and therefore no FRET signal is recorded (Figure 1).

We first evaluated the efficiency and selectivity of the FRET assay in microtiter plates using three different sample mixtures: (1) a mix of both FRET reaction probe molecules and the mouse anti-c-myc mAb (primary Ab) secreted by 9E10 hybridoma cells (positive sample), (2) a mix of both FRET reaction probe molecules and the mouse anti-human IFN-γ mAb (non-specific Ab) secreted by 7R2/A4 hybridoma cells (negative sample), and (3) a mix of both probe molecules without mAbs (reference sample). Emission spectra were recorded on a spectrofluorometer using an excitation wavelength at 488 nm. As expected, only in the presence of the anti-c-myc antibody, an FRET signal is detected (with peak emission at 668 nm; Figure 1), hence confirming that the antibody-binding assay is highly specific.

Cells remain viable and functional in droplets over extended period of time

Once the selectivity of the FRET assay was established, we evaluated the viability of individual hybridoma cells in 40 pl volume microfluidic droplets. Owing to the finite amount of nutrients available in each droplet and the gradual accumulation of waste products, the encapsulated cells will terminate their metabolic functions after a period of time defined by the droplet volume. To determine whether or not the hybridoma cells remain viable during both the on-chip and off-chip procedures necessary for completing the screening process, we first encapsulated 9E10 cells in 40 pl droplets containing RPMI-1640 growth media supplemented with 10% FBS and 16% (v/v) Optiprep using a cell encapsulation device (Figure S1A and Data S2). The emulsion was then incubated at 37°C/5% CO_2 and at selected time points during the incubation period, cells were released from the droplets by chemically breaking the emulsion, and then stained with 0.5% (w/v) trypan blue dye to evaluate their viability and integrity. Although most of the encapsulated cells died after overnight incubation, approximately 90% of all cells remained viable during the first 9 h (Figure S2). This represents a sufficiently long period of time for performing all required microfluidic operations, and largely agrees with previous cell viability studies in microdroplets (Periyannan Rajeswari et al., 2017). In addition, we confirmed that encapsulated cells released from the droplets after 3 h of incubation

could be cultured in a 96-well microtiter plate for 7 days, demonstrating excellent recovery, with ~92% of released cells proliferating *in vitro* (see STAR Methods). Based on these results, we concluded that the functional hybridoma cell assay could be conducted in 40 pl droplets within a 3–9 h time-window, without adverse effects on cell viability.

Next, we evaluated antibody secretion by individual 9E10 hybridoma cells. We encapsulated cells with culture media and the FRET reaction probes and measured Ab levels by recording fluorescence emission at wavelengths above 655 nm. As expected, the FRET signal of "positive" droplets such as those containing a cell, increased over time, with the signal from droplets containing no cells remaining at background levels (Figure 2). We used a custom-written image analysis script in Matlab to quantify the secreted and membrane-bound antibody fractions produced by individual cells (Figure S3 and Data S1). By recording FRET signal over a 60-min period, we observed secretion kinetics which are best described by a two-step process: a 3-fold increase in secreted antibody levels was observed from 0 to 15 min, at a rate of 1.18 nM/min, followed by a 1.6-fold increase in secreted antibody levels observed from 15 to 60 min, at a rate of 0.38 nM/min (Figure 2C). These results suggest that in our droplet-based assay a significant fraction of intracellular antibody is released rather quickly, presumably due to the sudden temperature shift, since the cells were collected at 4°C and assayed at 37°C. Incubation for periods longer than 1 h did not increase (or diminish) the overall number of secreting cells or the number of positive droplets. By titrating the soluble Ab levels in droplets (Figure S4), we estimated that a single encapsulated 9E10 hybridoma cell secretes ~800'000 Ab molecules, on average, in a 60-min interval, at a rate of ~14'000 Abs/min (Tables S1 and S2). Therefore, nanomolar concentrations of secreted Abs are achieved in just 15 min. Given the observed Ab secretion rates and picoliter-volumes of the droplets used, the FRET assay appears well suited for high-throughput screening and evaluation of secretion events. Interestingly, the average amount of membrane-bound antibody remained constant over the course of the experiment, at approximately 78'000 $\pm$ 23'000 mAb molecules per cell, or roughly 100 IgG/μm^2 (Figure 2D), implying that the fluorescence signal emanating from the cell surface does not provide a straightforward proxy for Ab secretion levels. It is worth noting, however, that our assay format does not differentiate whether membrane-associated Abs are being continuously recycled, or remain stably associated with the membrane. Nonetheless, our results are consistent with previous reports showing that mouse hybridoma cells simultaneously express both the membrane-bound and secreted forms of immunoglobulins. The ratio between the two fractions may depend on alternative RNA splicing (Helman et al., 2014; Liu et al., 2015; Pogson et al., 2016), physiological cell state (Charlet et al., 1995; Corrêa et al., 2016; Listek et al., 2020), transcriptional variability (Price et al., 2009; Shi et al., 2015), and cell cycle (Charlet et al., 1995; Kromenaker and Srienc, 1991).

Cell sorting and enrichment

Having confirmed that individual hybridoma cells isolated in 40 pl volume droplets produce sufficient quantities of antibodies for detection by FRET, we next sought to enrich the highest mAb producers from a heterogeneous mixture using a microfluidic FRET-activated droplet sorter (Figures 3, S1B, and Data S3). The droplet sorting platform was loosely based on our previous work (Mazutis et al., 2013) and optical components are detailed in Figure S3E. We first spiked 9E10 cells (0.1%) into a population of 7R2/A4 hybridoma cells, with the resulting heterogeneous mixture then being encapsulated along with cell growth medium and both FRET detection probes. To enable visual differentiation between the two cell types, the 7R2/A4 cells were stained with Hoechst 33,342 dye, the emission of which does not interfere with our FRET assay. Single-cell encapsulation was performed using a 30 μm deep flow-focusing geometry at an average rate of 600 cells s^{-1} (Figure S1A and Video S1). The encapsulated cells were incubated off-chip for 30 min to allow Ab secretion to occur and then sorted for 2 h using a microfluidic sorter at a rate of approximately 500 events s^{-1} (Figure S1B and Video S2). The fluorescence profiles of each droplet passing the interrogation point were recorded using photomultiplier tubes and analyzed using a custom-built LabVIEW program. In the event that the recorded FRET signal crosses a predefined sorting threshold, an electric pulse is generated, inducing a dipole moment within the passing aqueous droplet and pulling it into the sorting channel (Video S2). Droplets containing no cell or cells producing a non-specific antibody were not sorted and passively collected into the waste channel (Video S2). As expected, most droplets containing a cell did not produce an FRET signal due to lack of the specific antibody required for FRET to occur (Figure 3B). Only a small fraction of droplets (~0.01%–0.03%) showed distinguishable FRET acceptor emission indicating the presence of anti-c-myc-secreted antibodies and specific binding events (Figure 4A).

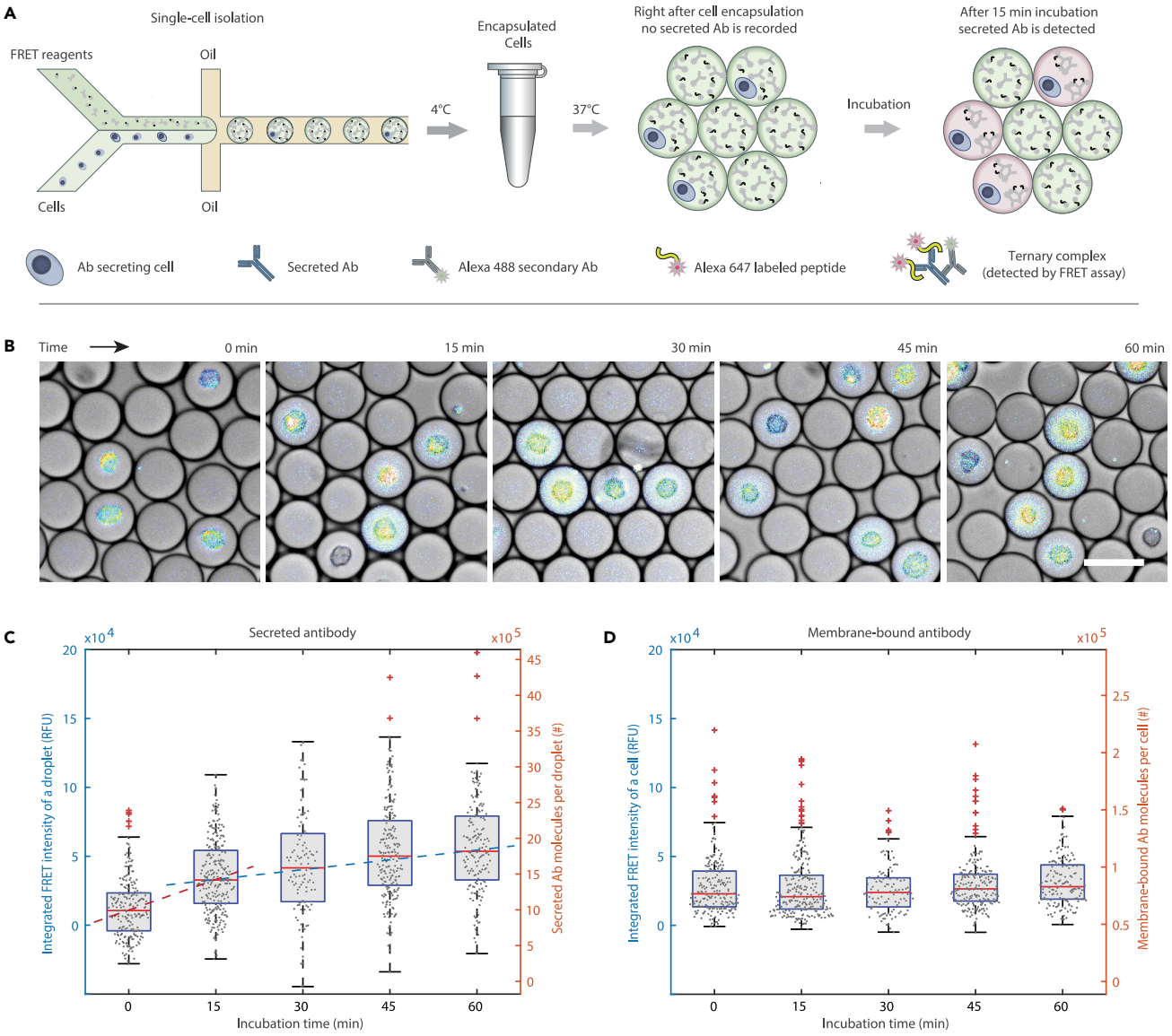

Figure 2. Single-cell antibody secretion assay in droplets using FRET

(A) The schematics of the FRET-based assay. The assay mix containing cell growth medium, Alexa Fluor 488-labeled secondary antibody (FRET donor), Alexa Fluor 647-labeled c-myc peptide (FRET acceptor) are encapsulated in 40 pl droplets along with anti-c-myc antibody-secreting 9E10 hybridoma cells (blue). Following incubation off-chip at 37°C, the secreted and membrane-bound antibody fractions are recorded using FRET (emission from Alexa Fluor 647). In the presence of the antibody, the two labeled probe molecules form a ternary complex enabling the FRET reaction to occur.

(B) Images of droplets acquired during 60 min of incubation using a widefield fluorescence microscope. The fluorescence intensity is color-coded, with red color pixels indicating the highest fluorescence intensity and blue the lowest. Scale bar, 50 μm.

(C) FRET acceptor fluorescence intensity of droplets as a function of time. A clear increase in droplet fluorescence intensity (with a slope of 1.18 nM/min - red dashed line, and with a slope of 0.38 nM/min - blue dashed line) over time is observed, indicating the accumulation of the secreted antibody of interest.

(D) The FRET acceptor fluorescence intensity of encapsulated cells. Cell fluorescence emanating from antibodies displayed at the cell membrane remains relatively stable over time. In panels C and D, the Y axes indicate the integrated FRET intensity subtracted by the average background FRET signal of droplets having no cells. Boxplots in C and D show the median (red lines) with upper and lower quartiles (blue lines), bars indicate the extremes of the distribution and crosses indicate outliers. See also Figures S3 and S4.

The droplets with the highest FRET signal were sorted into the collection tube and inspected through both bright-field and fluorescence microscopy. Analysis revealed that prior to sorting only 0.12% of all productive-droplets contained a target cell, while after sorting the fraction containing a cell of interest increased to 99.12% (Figure 3B). Repeating the microfluidic sorting procedure with a fresh mixture of cells produced

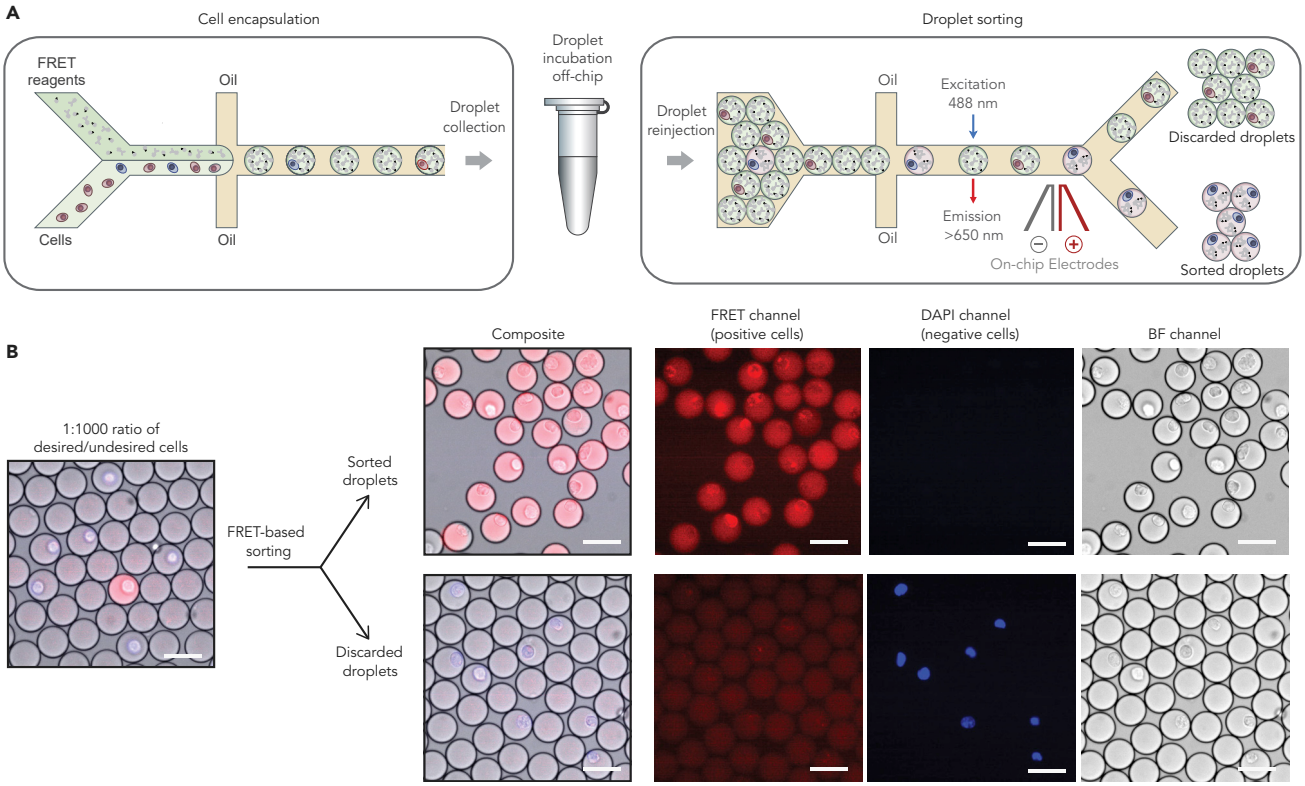

Figure 3. Sorting of FRET-positive droplets to isolate cells secreting target-reactive antibodies

(A) The schematics of the cell sorting based on antibody secretion. The assay mix containing cell growth medium, Alexa Fluor 488-labeled secondary antibody (FRET donor), and Alexa Fluor 647-labeled c-myc peptide (FRET acceptor) is encapsulated together with a mixture of hybridoma cells. The anti-c-myc antibody-secreting 9E10 cells are marked in blue, and the non-specific, anti-IFN-γ antibody-secreting 7R2/A4 cells are marked in dark red. The collected droplets are incubated off-chip at 37°C to induce antibody secretion and then re-introduced into the microfluidic droplet-sorting device for sorting based on the red FRET acceptor fluorescence signal (emission from Alexa Fluor 647). In the absence of the antigen-specific antibody, the acceptor molecule is not bound and therefore not excited upon illumination with the 488 nm laser. Thus, only emission from the green FRET donor is observed. In the presence of the desired antibody (blue), the two labeled probe molecules form a ternary complex and the FRET donor and acceptor molecules are brought in closeness, proximity, enabling the FRET reaction to occur. In this case, in addition to the green FRET donor emission, red light is emitted by the FRET acceptor molecule.

(B) Digital micrographs of droplets before and after FRET-based sorting. Before sorting, the desired cells (red) are rare, such that no strong FRET signal is observed with the majority of encapsulated cells displaying the Hoechst 33,342 stain (blue), identifying these cells as undesired 7R2/A4 cells. After sorting, a significant enrichment of desired cells is observed. The discarded fraction mostly consists of droplets containing the undesired cell type, or no cell. Scale bars, 50 μm. See also Figures S3 and S5.

similar results: the fraction of droplets with a positive cell after one round of sorting increased from 0.11% to 95.79%. These results in turn correspond to 827 ± 15-fold enrichment of cells secreting the desired antigen-specific antibody, with the main source of false positives being random co-encapsulation of negative and positive cells within the same droplet, or occasional splitting of droplets at the sorting junction. As expected, the droplets collected in the waste channel showed FRET signal at the background level (Figures 3B and S5). Hence, any cell that does not produce specific antibody is efficiently discarded by the FRET-based droplet sorting process.

Importantly, a unique feature of the developed droplet-based FRET assay is that the fluorescence profile of each droplet provides a footprint of the functional phenotypic state of the compartmentalized cell. When a cell secretes antibody molecules into the droplet milieu (e.g., a cell is an efficient mAb secretor), the fluorescence profile of a droplet shows an elevated FRET signal over the entire droplet volume (Figure 4B). On the other hand, if the cell happens to be a poor secretor with most Ab remaining associated with the membrane, the FRET signal will generate a characteristic, narrow fluorescence peak (Figure 4C). Accordingly, cells expressing either membrane-bound or secreted antibody fractions, or both, can be efficiently differentiated and sorted (Figures 4B–4D). Cells that secrete an irrelevant antibody displayed low fluorescence (Figure 4E).

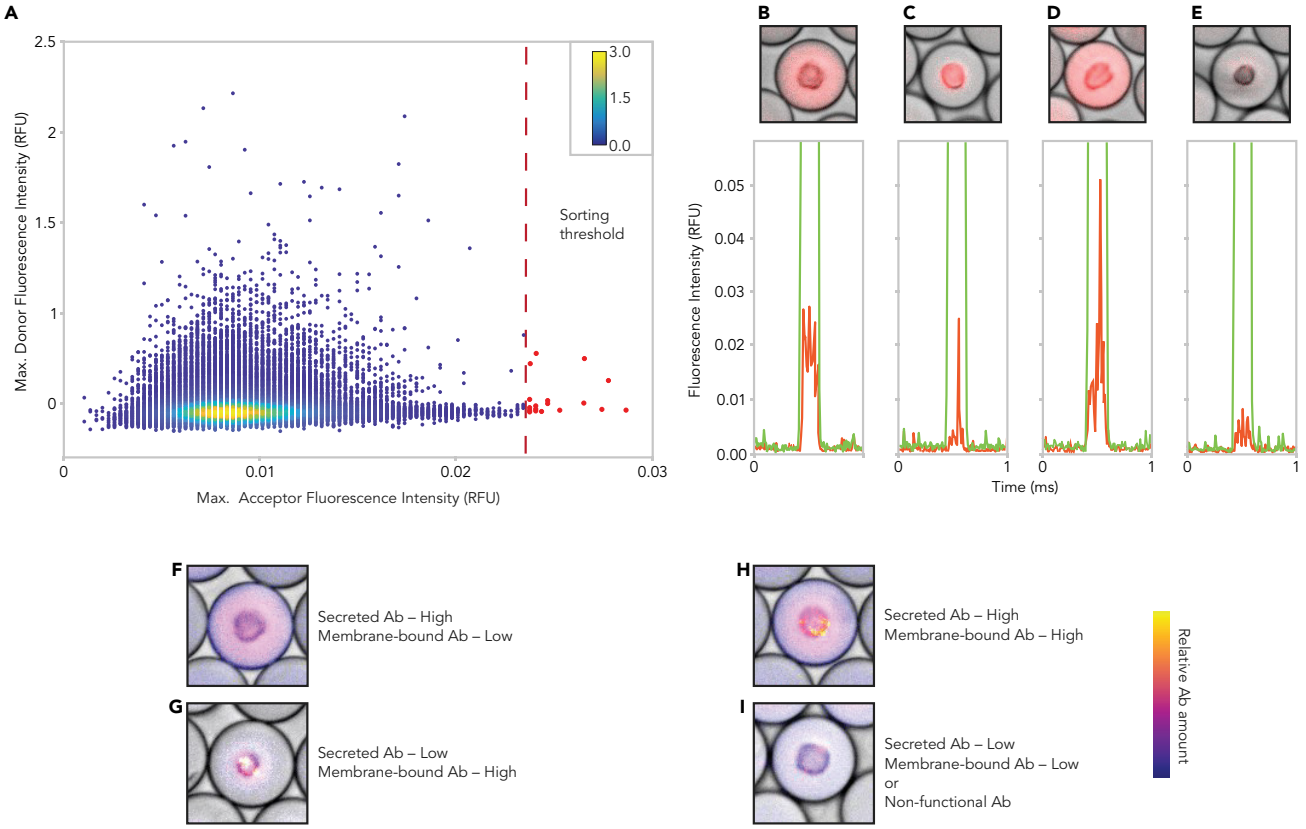

Figure 4. Time traces and scatterplot of FRET signal during microfluidic sorting

(A) Relative maximum donor/acceptor fluorescence signals recorded during the sorting process. The red dashed line represents the chosen sorting threshold, with sorted droplets indicated by red dots. Color bar indicates droplet number in log scale.

(B–E) Representative fluorescence time traces recorded throughout the sorting experiment. Both FRET donor fluorescence (green) and FRET acceptor fluorescence (red) are recorded. All droplets show strong donor fluorescence, allowing direct detection of each droplet. The FRET acceptor fluorescence intensity originating from positive droplets depends on Ab expression by individual cells. Droplets containing cells that secrete a large amount of target-reactive Ab display an elevated fluorescence pedestal (B), while those bearing cells with primarily membrane-bound target-reactive Ab are characterized by a narrow fluorescence peak (C). Cells that produce both secreted and membrane-bound forms of target-reactive Ab are characterized by an elevated fluorescence pedestal with a narrow fluorescence peak (D). Empty droplets and those containing cells that secrete an irrelevant Ab display low fluorescence in the red channel (E).

(F–I) Selected examples of color-coded droplets containing: a cell secreting large quantities of target-reactive Ab and producing only a small amount of membrane-associated Ab (F); a cell producing high levels of membrane-bound Ab (G); a cell producing high quantities of both, secreted and membrane-bound Ab fractions (H); and a cell showing reduced levels of Ab expression and/or cell producing unreactive (non-functional) Ab (I).

Finally, to confirm that sorted cells indeed maintain physiological and antibody secretion functions, we sorted and collected 624 droplets based on FRET intensity. The sorted cells were released into a 24-well cell culture plate, and after 12 days of culturing, the IgG levels in the supernatant were evaluated through a standard ELISA assay. Prior to sorting, the artificial mix of hybridoma cells produced a large amount of anti-IFN-γ antibody (97.05% of all antibodies), and only a small fraction of the desired anti c-myc antibody (2.95%). However, after sorting, anti c-myc antibody production became dominant (98.85% of all antibodies, Figure 5). These results confirm that the developed FRET-based single-cell antibody secretion assay provides excellent specificity, and in combination with microfluidic sorting, enables high-throughput enrichment for rare cells of interest while maintaining their viability and physiological functions.

DISCUSSION

Conventional approaches for high-throughput screening of single cells for functional activity often rely on FACS. Although successful in certain experimental settings, FACS-based approaches are largely restricted to sorting of individual cells based on intracellular or membrane-bound epitope staining. Screening of

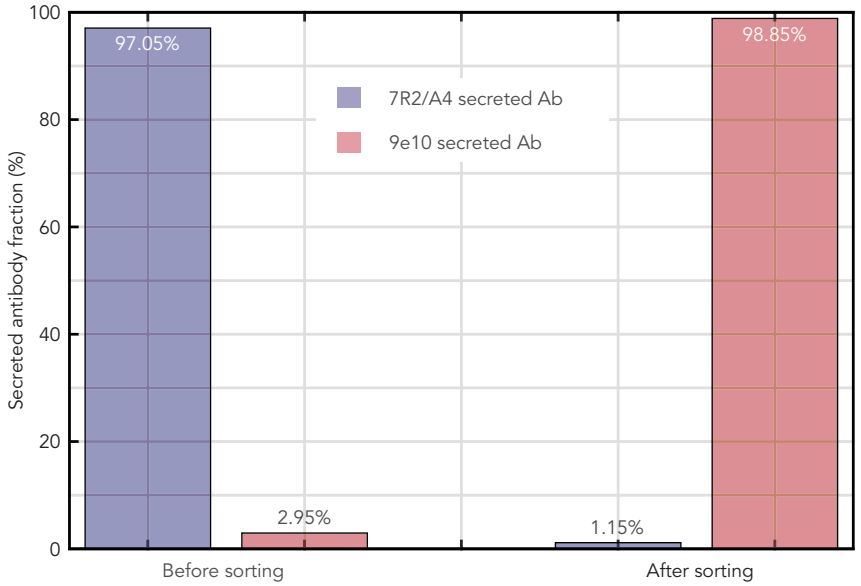

Figure 5. Antibody binding evaluation by ELISA, before and after droplet sorting

Columns represent the measured antibody fraction from the heterogeneous cell population before and after FRET-based sorting. Prior to sorting, a mixture of 7R2/A4 and 9E10 cells was incubated for 24 h and the supernatant was collected. ELISA was performed to determine the reactivity of the antibody mixture against c-myc peptide and IFN-γ. The mixture of cells was then washed in fresh media and encapsulated, and droplets showing high anti-c-myc FRET signal were sorted. Collected cells (n = 624) were released from droplets, cultured for 12 days, and the supernatant tested for reactivity against c-myc and IFN-γ. The undesired anti IFN-γ antibodies secreted by 7R2/A4 cells (violet) accounted for most of the ll secreted antibodies. However, after one round of sorting, the majority of antibodies were the desired anti-c-myc antibody (coral), secreted by 9E10 cells, indicating efficient sorting and specificity of the presented FRET-assay. Data shown as absolute value.

individual cells based on the activity of secreted proteins is a much more challenging task, as the secreted biomolecules (e.g., antibodies) do not remain physically associated with the cell producing them; hence, the genotype-phenotype linkage is lost. Single-cell compartmentalization using microfluidics provides an appealing option for capturing and quantifying the secreted antibodies (Debs et al., 2012; Dressler et al., 2014; Eyer et al., 2017; Fitzgerald et al., 2015; Jin et al., 2009; Love et al., 2006; Mazutis et al., 2013; Rakszewska et al., 2014; Shembekar et al., 2016; Singhal et al., 2010), and for establishing a link between the cellular phenotype and genotype (An et al., 2017; Bounab et al., 2020; Chen et al., 2016; Ding et al., 2020; Gérard et al., 2020; Lu et al., 2015; Zhou et al., 2020).

In this work, we report a droplet-based microfluidic platform for screening and sorting antibody-secreting cells based on FRET signal. One of the distinctive characteristics of the single-cell FRET assay described here is the ability to simultaneously differentiate the secreted and membrane-bound antibody fractions produced by individual droplet-encapsulated cells. Such analytical capabilities are lacking in most current microfluidic systems, despite being critically important for identification and selection of the cells that efficiently produce and secrete proteins. For example, the industrial production of therapeutic proteins such as antibodies relies on isolation of the individual clones that efficiently secrete the desired protein versus clones that display it on the membrane. The microfluidic platform based on FRET assay may facilitate the generation of functional cell lines that secrete high levels of functional protein of interest and may find many uses in biotechnology that require quantitative analysis and screening of heterogeneous cell populations.

The developed platform also offers several other advantages. In contrast to a fluorescent bead-based assay (Mazutis et al., 2013), where cell screening is limited by the bead (carrying a ligand) and target cell co-encapsulation events, the approach reported here circumvents the fundamental constraints imposed by Poisson encapsulation. Because the FRET-assay reagents are uniformly distributed in all droplets, each compartmentalized cell can be interrogated and sorted in a high-throughput manner according to the

phenotypic state. As with many other miniaturized assays (Guo et al., 2012), compartmentalization of single cells in microdroplets significantly reduces the assay time. For instance, we determined that the immunoglobulin secretion rate of individual mouse hybridoma 9E10 cells is ~200 IgG/sec, suggesting that a detectable (nanomolar-range) concentration of secreted antibodies in a picoliter-volume droplet will be reached within a 1-h window. Indeed, we found that by isolating hybridoma cells in 40 pl droplets, a sufficiently high FRET signal of immunoassay is reached in only 15 to 30 min; in contrast, an analogous assay in microtiterplate would take 1–3 days.

Performing the antibody secretion assay over the course of 1 h, we found that the Ab secretion levels varied broadly between individual cells (~190'000 ± 80'000 molecules), while the membrane-associated Ab fraction quickly saturated at ~78'000 ± 23'000 Abs per single cell. Intracellular Ab staining by the detection probes can be ruled out due to the relatively high molecular weight of the FRET assay components that would need to be engulfed by live cells. Our results, in corroboration with those of others (Debs et al., 2012; Eyer et al., 2017), suggest that despite being derived from a single clone, the expansion of hybridoma cells in culture leads to a phenotypically diverse population composed of cell-secretors that secrete a significant part of their total Ab fraction, cell-producers whose secreted Ab fraction is substantially smaller compared to the membrane-bound fraction, and inactive or suppressed cells for which Ab synthesis remains negligible.

Finally, to expand the scope of applications, we performed FRET-based microfluidic sorting to enrich cells producing the highest levels of functional antibody and showed that the developed platform offers sorting efficiencies of up to 97.5% at a rate of 200 cells s^{-1}, and achieved an 800-fold enrichment of antigen-specific antibody-secreting cells in only one round of sorting. Sorted cells were retrieved from the droplets and successfully expanded in cell culture, indicating that all the microfluidic processing steps are compatible with live-cell screening and enrichment. Overall, we anticipate that the presented FRET-based assay in combination with droplet microfluidics offers a broad application potential and will add to the collection of microfluidic tools for the detection of secreted cellular proteins, as well as the screening and sorting of antibody-secreting primary B cells, or large recombinant ASC libraries.

Limitations of the study

Besides providing clear analytical advantages for identifying the functional cell phenotypes, the FRET technique reported here is not without limitations. The assay is built on fluorescence readout and multiple factors are known to affect the quality of signal (Lichtman and Conchello, 2005). The FRET signal is mediated by the binding of target antibody to donor and acceptor probes, and since the excited donor either fluoresces or transfers energy to the acceptor dye, the FRET efficiency is inherently sensitive to inter-dye distance (Roy et al., 2008). Consequently, obtaining the fluorescently labeled antigen of interest, which upon binding the Ab would be brought into closeness, proximity (Förster distance) to a fluorescently labeled secondary antibody, may be a nontrivial task. On the other hand, combining two fluorescently labeled secondary antibodies recognizing different epitopes on the same target, the individual cells secreting cytokines, chemokines, or other proteins of interest could be efficiently interrogated and their real-time secretion dynamics evaluated.

Conducting protein secretion assay in water-in-oil droplets reduces the assay time significantly. However, given the finite amount of nutrients available inside the microdroplets, the cell viability over longer periods of time (>9h) deteriorates and should be carefully considered when working with primary cells that may exhibit slower secretion kinetics. Another limitation is sorting throughput. Cell sorting speed of the microfluidic system reported here is at least an order of magnitude slower than a conventional FACS instrument, at the trade-off of lower shear forces applied to the cells, and high sorting purity. However, as the scope of single-cell methods continues to grow, the analytical benefits offered by the FRET-based single-cell screening platform should outweigh these few constraints and enable the quantitative high-throughput characterization and enrichment of desirable phenotypes.

STAR★METHODS

Detailed methods are provided in the online version of this paper and include the following:

- KEY RESOURCES TABLE
- RESOURCE AVAILABILITY
  - Lead contact

SUPPLEMENTAL INFORMATION

Supplemental information can be found online at https://doi.org/10.1016/j.isci.2022.104515.

ACKNOWLEDGMENTS

J.R. is particularly grateful to Dirk van Swaay (Wunderlichips GmbH) for sharing valuable knowledge about microfabrication and surface treatment techniques. J.R. received a fellowship from Sciex-NMS^{ch} – Scientific Exchange Programme between Switzerland and the New Member States of the European Union. This work was supported by the European Social Fund (project No. 09.3.3-LMT-K-712-01-0056) under grant agreement with the Research Council of Lithuania. The work in A.D. group was supported by ETH Zürich.

AUTHOR CONTRIBUTIONS

Conceptualization, L.M. and J.H.; Methodology, J.R., S.S., J.H., and L.M.; Software, O.D. and S.B.; Formal Analysis, J.R., S.B., and L.M.; Investigation, J.R.; Writing – Original Draft, J.R. and L.M.; Writing – Review & Editing, J.R., S.B., J.H., X.C.S., A.dM., and L.M.; Supervision, X.C.S., A.dM., and L.M.; Funding Acquisition, A.dM. and L.M.

DECLARATION OF INTERESTS

The authors declare no competing interests.

Received: June 21, 2021
Revised: November 5, 2021
Accepted: May 29, 2022
Published: July 15, 2022

REFERENCES

Akbari, S., and Pirbodaghi, T. (2014). A droplet-based heterogeneous immunoassay for screening single cells secreting antigen-specific antibodies. Lab Chip *14*, 3275–3280. 101039/C4LC00082J.

An, X., Sendra, V.G., Liadi, I., Ramesh, B., Romain, G., Haymaker, C., Martinez-Paniagua, M., Lu, Y., Radvanyi, L.G., Roysam, B., et al. (2017). Single-cell profiling of dynamic cytokine secretion and the phenotype of immune cells. PLoS One *12*, e0181904. https://doi.org/10.1371/journal.pone.0181904.

Auner, H.W., Beham-Schmid, C., Dillon, N., and Sabbattini, P. (2010). The life span of short-lived plasma cells is partly determined by a block on activation of apoptotic caspases acting in combination with endoplasmic reticulum stress. Blood *116*, 3445–3455. https://doi.org/10.1182/blood-2009-10-250423.

Azizi, A., Arora, A., Markiv, A., Lampe, D.J., Miller, T.A., and Kang, A.S. (2012). Ribosome display of combinatorial antibody libraries derived from mice immunized with heat-killed Xylella fastidiosa and the selection of MopB-specific single-chain antibodies. Appl. Environ. Microbiol. *78*, 2638–2647. https://doi.org/10.1128/aem.07807-11.

Bounab, Y., Eyer, K., Dixneuf, S., Rybczynska, M., Chauvel, C., Mistretta, M., Tran, T., Aymerich, N., Chenon, G., Llitjos, J.-F., et al. (2020). Dynamic single-cell phenotyping of immune cells using the microfluidic platform DropMap. Protoc *15*, 2920–2955. https://doi.org/10.1038/s41596-020-0354-0.

Chan, J.C., and Chan, A.T. (2017). Biologics and biosimilars: what, why and how? ESMO Open *2*, e000180. https://doi.org/10.1136/esmoopen-2017–20000180.

Chan, C.E.Z., Lim, A.P.C., MacAry, P.A., and Hanson, B.J. (2014). The role of phage display in therapeutic antibody discovery. Int. Immunol. *26*, 649–657. https://doi.org/10.1093/intimm/dxu082.

Charlet, M., Kromenaker, S.J., and Srienc, F. (1995). Surface IgG content of murine hybridomas: direct evidence for variation of antibody secretion rates during the cell cycle. Biotechnol. Bioeng. *47*, 535–540. https://doi.org/10.1002/bit.260470505.

Chen, B., Lim, S., Kannan, A., Alford, S.C., Sunden, F., Herschlag, D., Dimov, I.K., Baer, T.M., and Cochran, J.R. (2016). High-throughput analysis and protein engineering using microcapillary arrays. Nat. Chem. Biol. *12*, 76–81. https://doi.org/10.1038/nchembio.1978.

Cocco, M., Stephenson, S., Care, M.A., Newton, D., Barnes, N.A., Davison, A., Rawstron, A., Westhead, D.R., Doody, G.M., and Tooze, R.M. (2012). *In vitro* generation of long-lived human plasma cells. J. Immunol. *189*, 5773–5785. https://doi.org/10.4049/jimmunol.1103720.

Cooper, M.D., Peterson, R.D., and Good, R.A. (1965). Delineation of the thymic and bursal lymphoid systems in the chicken. Nature *205*, 143–146. https://doi.org/10.1038/205143a0.

Corrêa, A.L., Senna, J.P.M., and de Sousa, Á.P.B. (2016). Effects of passage number on growth and productivity of hybridoma secreting MRSA anti-PBP2a monoclonal antibodies. Cytotechnology *68*, 419–427. https://doi.org/10.1007/s10616-014-9794-0.

Debs, B.E., Utharala, R., Balyasnikova, I.V., Griffiths, A.D., and Merten, C.A. (2012). Functional single-cell hybridoma screening using droplet-based microfluidics. Proc. Natl. Acad. Sci. USA *109*, 11570–11575. https://doi.org/10.1073/pnas.1204514109.

Ding, R., Hung, K.-C., Mitra, A., Ung, L.W., Lightwood, D., Tu, R., Starkie, D., Cai, L., Mazutis, L., Chong, S., et al. (2020). Rapid isolation of antigen-specific B-cells using droplet microfluidics. RSC Adv. *10*, 27006–27013. https://doi.org/10.1039/d0ra04328a.

Drabek, D., Janssens, R., de Boer, E., Rademaker, R., Kloess, J., Skehel, J., and Grosveld, F. (2016). Expression cloning and production of human heavy-chain-only antibodies from murine transgenic plasma cells. Front. Immunol. *7*, 619. https://doi.org/10.3389/fimmu.2016.00619.

Dressler, O.J., Maceiczyk, R.M., Chang, S.-I., and deMello, A.J. (2014). Droplet-based microfluidics: enabling impact on drug discovery. J. Biomol. Screen *19*, 483–496. https://doi.org/10.1177/1087057113510401.

Eyer, K., Doineau, R.C.L., Casterillon, C.E., Briseño-Roa, L., Menrath, V., Mottet, G., England, P., Godina, A., and Brient-Litzler, E. (2017). Single-cell deep phenotyping of IgG-secreting cells for high-resolution immune monitoring. Nat. Biotechnol. *35*, 977–982. https://doi.org/10.1038/nbt.3964.

Fischer, N. (2011). Sequencing antibody repertoires: the next generation. mAbs *3*, 17–20. https://doi.org/10.4161/mabs.3.1.14169.

Fitzgerald, V., Manning, B., O'Donnell, B., O'Reilly, B., O'Sullivan, D., O'Kennedy, R., and Leonard, P. (2015). Exploiting highly ordered subnanoliter volume microcapillaries as microtools for the analysis of antibody producing cells. Anal. Chem. *87*, 997–1003. https://doi.org/10.1021/ac503547j.

Frenzel, A., Hust, M., and Schirrmann, T. (2013). Expression of recombinant antibodies. Immunol. *4*, 217. https://doi.org/10.3389/fimmu.2013.00217.

Frenzel, A., Kügler, J., Helmsing, S., Meier, D., Schirrmann, T., Hust, M., and Dübel, S. (2017). Designing human antibodies by phage display. Transfus. Med. Hemotherapy *44*, 312–318. https://doi.org/10.1159/000479633.

Gérard, A., Woolfe, A., Mottet, G., Reichen, M., Castrillon, C., Menrath, V., Ellouze, S., Poitou, A., Briseno-Roa, L., Canales-Herrerias, P., et al. (2020). High-throughput single-cell activity-based screening and sequencing of antibodies using droplet microfluidics. Nat. Biotechnol. *38*, 715–721. https://doi.org/10.1038/s41587-020-0466-7.

Gitlin, A.D., Mayer, C.T., Oliveira, T.Y., Shulman, Z., Jones, M.J.K., Koren, A., and Nussenzweig, M.C. (2015). T cell help controls the speed of the cell cycle in germinal center B cells. Science *349*, 643–646. https://doi.org/10.1126/science.aac4919.

Guo, M.T., Rotem, A., Heyman, J.A., and Weitz, D.A. (2012). Droplet microfluidics for high-throughput biological assays. Lab Chip *12*, 2146. https://doi.org/10.1039/c2lc21147e.

Helman, D., Toister-Achituv, M., Bar-Shimon, M., Cohen, B., Otmi, I., Berger, N., Kalimi, D., Kimalov, B., Medina, T., Sapir, A., et al. (2014). Novel membrane-bound reporter molecule for sorting high producer cells by flow cytometry: membrane-Bound Reporter for Sorting High Producer Cells. Cytometry *85*, 162–168. https://doi.org/10.1002/cyto.a.22308.

Jin, A., Ozawa, T., Tajiri, K., Obata, T., Kondo, S., Kinoshita, K., Kadowaki, S., Takahashi, K., Sugiyama, T., Kishi, H., and Muraguchi, A. (2009). A rapid and efficient single-cell manipulation method for screening antigen-specific antibody–secreting cells from human peripheral blood. Med *15*, 1088–1092. https://doi.org/10.1038/nm.1966.

Josephides, D., Davoli, S., Whitley, W., Ruis, R., Salter, R., Gokkaya, S., Vallet, M., Matthews, D., Benazzi, G., Shvets, E., et al. (2020). Cyto-mine: an integrated, picodroplet system for high-throughput single-cell analysis, sorting, dispensing, and monoclonality assurance. Transl. Life Sci. Innov *25*, 177–189. https://doi.org/10.1177/2472630319892571.

Kromenaker, S.J., and Srienc, F. (1991). Cell-cycle-dependent protein accumulation by producer and nonproducer murine hybridoma cell lines: a population analysis. Biotechnol. Bioeng. *38*, 665–677. https://doi.org/10.1002/bit.260380612.

Lichtman, J.W., and Conchello, J.-A. (2005). Fluorescence microscopy. Nat. Methods *2*, 910–919. https://doi.org/10.1038/nmeth817.

Listek, M., Hönow, A., Gossen, M., and Hanack, K. (2020). A novel selection strategy for antibody producing hybridoma cells based on a new transgenic fusion cell line. Sci. Rep. *10*, 1664. https://doi.org/10.1038/s41598-020-58571-w.

Liu, J.K.H. (2014). The history of monoclonal antibody development – progress, remaining challenges and future innovations. Ann. Med. Surg *3*, 113–116. https://doi.org/10.1016/j.amsu.2014.09.001.

Liu, H., White, J., Crawford, F., Jin, N., Ju, X., Liu, K., Jiang, C., Marrack, P., Zhang, G., and Kappler, J.W. (2015). A rapid method to characterize mouse IgG antibodies and isolate native antigen binding IgG B cell hybridomas. PLoS One *10*, e0136613. https://doi.org/10.1371/journal.pone.0136613.

Love, J.C., Ronan, J.L., Grotenbreg, G.M., van der Veen, A.G., and Ploegh, H.L. (2006). A microengraving method for rapid selection of single cells producing antigen-specific antibodies. Nat. Biotechnol. *24*, 703–707. https://doi.org/10.1038/nbt1210.

Lu, R.-M., Hwang, Y.-C., Liu, I.-J., Lee, C.-C., Tsai, H.-Z., Li, H.-J., and Wu, H.-C. (2020). Development of therapeutic antibodies for the treatment of diseases. J. Biomed. Sci. *27*, 1. https://doi.org/10.1186/s12929-019-0592-z.

Lu, Y., Xue, Q., Eisele, M.R., Sulistijo, E.S., Brower, K., Han, L., Amir, E.a.D., Pe'er, D., Miller-Jensen, K., and Fan, R. (2015). Highly multiplexed profiling of single-cell effector functions reveals deep functional heterogeneity in response to pathogenic ligands. Proc. Natl. Acad. Sci. USA *112*, E607–E615. https://doi.org/10.1073/pnas.1416756112.

Mazutis, L., Gilbert, J., Ung, W.L., Weitz, D.A., Griffiths, A.D., and Heyman, J.A. (2013). Single-cell analysis and sorting using droplet-based microfluidics. Nat. Protoc. *8*, 870–891. https://doi.org/10.1038/nprot.2013.046.

Nojima, T., Haniuda, K., Moutai, T., Matsudaira, M., Mizokawa, S., Shiratori, I., Azuma, T., and Kitamura, D. (2011). In-vitro derived germinal centre B cells differentially generate memory B or plasma cells in vivo. Nat. Commun. *2*, 465. https://doi.org/10.1038/ncomms1475.

Pasqualini, R., and Arap, W. (2004). Hybridoma-free generation of monoclonal antibodies. Proc. Natl. Acad. Sci. U S A *101*, 257–259. https://doi.org/10.1073/pnas.0305834101.

Periyannan Rajeswari, P.K., Joensson, H.N., and Andersson-Svahn, H. (2017). Droplet size influences division of mammalian cell factories in droplet microfluidic cultivation: microfluidics and miniaturization. Electrophoresis *38*, 305–310. https://doi.org/10.1002/elps.201600316.

Pogson, M., Parola, C., Kelton, W.J., Heuberger, P., and Reddy, S.T. (2016). Immunogenomic engineering of a plug-and-(dis)play hybridoma platform. Nat. Commun. *7*, 12535. https://doi.org/10.1038/ncomms12535.

Price, P.W., McKinney, E.C., Wang, Y., Sasser, L.E., Kandasamy, M.K., Matsuuchi, L., Milcarek, C., Deal, R.B., Culver, D.G., and Meagher, R.B. (2009). Engineered cell surface expression of membrane immunoglobulin as a means to identify monoclonal antibody-secreting hybridomas. J. Immunol. Methods *343*, 28–41. https://doi.org/10.1016/j.jim.2009.01.005.

Rakszewska, A., Tel, J., Chokkalingam, V., and Huck, W.T. (2014). One drop at a time: toward droplet microfluidics as a versatile tool for single-cell analysis. NPG Asia Mater. *6*, e133. https://doi.org/10.1038/am.2014.86.

Roy, R., Hohng, S., and Ha, T. (2008). A practical guide to single-molecule FRET. Methods *5*, 507–516. https://doi.org/10.1038/nmeth.1208.

Seah, Y.F.S., Hu, H., and Merten, C.A. (2018). Microfluidic single-cell technology in immunology and antibody screening. Mol. Aspects Med *59*, 47–61. https://doi.org/10.1016/j.mam.2017.09.004.

Shembekar, N., Chaipan, C., Utharala, R., and Merten, C.A. (2016). Droplet-based microfluidics in drug discovery, transcriptomics and high-throughput molecular genetics. Lab Chip *16*, 1314–1331. https://doi.org/10.1039/c6lc00249h.

Shi, W., Liao, Y., Willis, S.N., Taubenheim, N., Inouye, M., Tarlinton, D.M., Smyth, G.K., Hodgkin, P.D., Nutt, S.L., and Corcoran, L.M. (2015). Transcriptional profiling of mouse B cell terminal differentiation defines a signature for antibody-secreting plasma cells. Nat. Immunol. *16*, 663–673. https://doi.org/10.1038/ni.3154.

Schneider, C.A., Rasband, W.S., and Eliceiri, K.W. (2012). NIH Image to ImageJ: 25 years of image analysis. Nat. Methods *9*, 671–675. https://doi.org/10.1038/nmeth.2089.

Singhal, A., Haynes, C.A., and Hansen, C.L. (2010). Microfluidic measurement of antibody–antigen binding kinetics from low-abundance samples and single cells. Anal. Chem. *82*, 8671–8679. https://doi.org/10.1021/ac101956e.

Smith, G.P. (1985). Filamentous fusion phage: novel expression vectors that display cloned antigens on the virion surface. Science *228*, 1315–1317. https://doi.org/10.1126/science.4001944.

Taccola, S., Greco, F., Sinibaldi, E., Mondini, A., Mazzolai, B., and Mattoli, V. (2015). Toward a new generation of electrically controllable hygromorphic soft actuators. Adv. Mater. *27*, 1668–1675. https://doi.org/10.1002/adma.201404772.

van Swaay, D., Tang, T.-Y.D., Mann, S., and de Mello, A. (2015). Microfluidic formation of membrane-free aqueous coacervate droplets in water. Angew. Chem. Int. Ed. *54*, 8398–8401. https://doi.org/10.1002/anie.201502886.

Zhou, Y., Shao, N., Bessa de Castro, R., Zhang, P., Ma, Y., Liu, X., Huang, F., Wang, R.-F., and Qin, L. (2020). Evaluation of single-cell cytokine secretion and cell-cell interactions with a hierarchical loading microwell chip. Cell Rep. *31*, 107574. https://doi.org/10.1016/j.celrep.2020.107574.

STAR★METHODS

KEY RESOURCES TABLE

REAGENT or RESOURCE	SOURCE	IDENTIFIER
Antibodies		
Goat polyclonal anti-mouse (Alexa Fluor®-488)	Jackson ImmunoResearch Laboratories, Inc., USA	Cat#115-545-006; RRID: AB_2338841
Anti-c-Myc antibody, clone 9E10	Millipore	Cat#MABE282; RRID: AB_11213164
Goat polyclonal anti-mouse (HRP)	BioLegend	Cat#405306; RRID: AB_315009
Chemicals, peptides, and recombinant proteins		
SU-8 3025	Kayaku Advanced Materials (formerly Micro-Chem)	Cat#NC0057282
Chlorotrimethylsilane	Sigma-Aldrich	Cat#92360; CAS: 75-77-4
SYLGARD™ 184 Silicone Elastomer Kit	Dow Corning	Cat#101697
(Tridecafluoro-1,1,2,2-tetrahydrooctyl) trichlorosilane, 97%	abcr GmbH	Cat#AB111444; CAS: 78560-45-9
3M™ Novec™ 7500 Engineered Fluid	3M	Cat#051243; CAS: 297730-93-9
5 wt % 008-FluoroSurfactant in HFE7500	RAN Biotechnologies	Cat#008-FluoroSurfactant-5wtH-20G
1H,1H,2H,2H-Perfluorooctan-1-ol	FluoroChem	Cat#007128; CAS: 647-42-7
TWEEN® 20	Sigma-Aldrich	Cat#P1379; CAS: 9005-64-5
Carbonate-Bicarbonate Buffer	Sigma-Aldrich	Cat#C3041
Non-fat-Dried Milk bovine	Sigma-Aldrich	Cat#M7409
3,3′,5,5′-Tetramethylbenzidine (TMB) Liquid Substrate System for ELISA	Sigma-Aldrich	Cat#T0440
Sulfuric Acid 10% pure	Panreac AppliChem	Cat#145882; CAS: 7664-93-9
RPMI 1640 Medium, no glutamine, no phenol red	Gibco	Cat#32404-014
Fetal bovine serum (FBS)	Gibco	Cat#26140-079
GlutaMAX™ Supplement	Gibco	Cat#35050-061
Penicillin-Streptomycin (10,000 U/mL)	Gibco	Cat#15140-122
DPBS	Gibco	Cat#14190-144
Trypan Blue Solution, 0.4%	Gibco	Cat#15250-061;
OptiPrep™ Density Gradient Medium	Sigma-Aldrich	Cat#D1556; CAS: 92339-11-2
NucBlue™Live ReadyProbes™ Reagent (Hoechst 33342)	Invitrogen	Cat#R37605
Human c-myc peptide (Alexa Fluor®-647)	JPT Peptide Technologies GmbH	EQKLISEEDL-Ttds–Cys(Alexa 647)
Human c-myc Peptide	Sigma-Aldrich	Cat#M2435
Human IFN-γ	Sigma-Aldrich	Cat#SRP3058
Deposited data		
Unprocessed data	Mendeley Data	https://doi.org/10.17632/k4sjbkcgt7.1
Experimental models: Cell lines		
Mouse: MYC 1-9E10.2 [9E10] hybridoma cells	ATCC	Cat#CRL-1729; RRID: CVCL_G671
Mouse: 7R2/A4 hybridoma cells	ECACC	Cat#92030601; RRID: CVCL_J052
Software and algorithms		
ImageJ	Schneider et al. (2012)	https://imagej.nih.gov/ij/
Droplet analysis algorithm	Supplementary Material	n/a

(*Continued on next page*)

Continued

REAGENT or RESOURCE	SOURCE	IDENTIFIER
LabView droplet sorter program (custom)	National Instruments	n/a
Adobe illustrator	https://www.adobe.com/	Version 25.0.1
MATLAB	https://ch.mathworks.com/products/matlab.html	R2019b
Other		
Silicon wafers	Siegert Wafer	Si-Wafer 4P0/>1/525 ± 25/SSP/TTV<10
High-resolution film mask	Micro Lithography Services Limited	n/a
UV exposure system	OAI	Model 30
Hole puncher	Syneo	Cat#CR0500355N18R4
Microscope coverslips	Thermo Scientific	Cat#11911998
Low-melting-temperature solder wire	The Indium Corporation of America	Cat#wirebn-53307
Wire	Alpha Wire	Cat#1560 RD005
Epoxy adhesives	Araldite	Cat#50635-00000
1 mL syringes	Omnifix	Cat#612-2899
PTFE Microtubing, 0.56 × 1.07 mm	Fischer Scientific	Cat#NC1729627
Syringe pump: Pump 11 Pico Plus Elite	Harvard Apparatus	Cat#70-4511
Aladdin SyringeONE Programmable Syringe Pumps	World Precision Instruments, Inc.	AL-1000
High-speed camera	Vision Research	Phantom Miro M310
Inverted microscope	Nikon	Nikon Ti-E
488 nm diode laser	Omicron-laserage Laserprodukte GmbH	PhoxX+ 488-100
Photomultiplier tubes (PMTs)	Hamamatsu Photonics	Cat# H10722-20
20x objective	Nikon	CFI S Plan Fluor ELWD ADM 20X
Field-programmable gate array (FPGA)	National Instruments	n/a
High voltage amplifier	Trek Inc.	Model 2201
Brightfield light source	CoolLED	pW-100
Fluorescence light source	Omicron	LedHUB® with up to 6 wavelengths
Fluorescence light source	Lumencor Inc.	Spectra-X LED Light Engine
Cylindrical lense	Thorlabs	Cat#LJ1558RM
Dichroic mirror, 505	AHF Analysentechnik	Cat#F33-505A
Dichroic mirror, 640	AHF Analysentechnik	Cat#F48-642
Notch filter, 491	AHF Analysentechnik	Cat#F57-640
Bandpass filter, 535/40	AHF Analysentechnik	Cat#F32-535A
Longpass filter, 655	AHF Analysentechnik	Cat#F47-655
Beam expander lens 1	Thorlabs	Cat#LA1509-A
Beam expander lens 2	Thorlabs	Cat#LA1805-A
Pinhole	Thorlabs	Cat#P40H
Fluorescence camera	PCO AG	pco.edge 5.5
sCMOS camera	Photometrics	Prime 95B
Spectrofluorometer	Horiba	FluoroMax-4
Nunc™ Cell-Culture Treated Multidishes	Thermo Scientific™	Cat#142485
Counting chamber, Fast Read® 102 |	Kova International	Cat#BVS100H
SecureSeal™ Hybridization Chambers	Grace Bio-Labs	Cat#621505
Thermo Scientific™ Nunc Micro-Well 96-Well Microplates, non-treated	Thermo Fisher Scientific	Cat#269620
Corning® 96 Well Half-Area Microplate	Sigma-Aldrich/Merck	Cat#CLS3694-100EA
Plate reader	Tecan	Infinite 200Pro

RESOURCE AVAILABILITY

Lead contact

Further information and requests for resources and reagents should be directed to the lead contact, Ph.D., Prof. Linas Mazutis (linas.mazutis@bti.vu.lt).

Materials availability

This study did not generate new unique reagents.

Data and code availability

Raw data reported in this paper is available at Mendeley Data: https://doi.org/10.17632/k4sjbkcgt7.1.

The code for the droplet fluorescence analysis is provided with this paper. Any additional information required to reanalyze the data reported in this paper is available from the lead contact upon request.

EXPERIMENTAL MODEL AND SUBJECT DETAILS

Cell lines

Mouse MYC 1-9E10.2 [9E10] hybridoma cells (ATCC: CRL-1729™; RRID: CVCL_G671), were obtained from the American Type Culture Collection. Sex of cells is not indicated by the provider. Cells were grown in Roswell Park Memorial Institute (RPMI) 1640 Medium, supplemented with 10% (v/v) fetal bovine serum (FBS), 2 mM GlutaMax, 100 units/mL penicillin, 100 μg/mL of streptomycin. Cells were cultured at 37°C, at 5% CO_2 in the air atmosphere. Cell concentration was maintained in a range of 1×10^5 and 1×10^6 cells/mL. Fresh, pre-warmed, complete RPMI-1640 growth medium was added 12 h before cell encapsulation.

Mouse 7R2/A4 hybridoma cells were purchased from the European Collection of Authenticated Cell Cultures (ECACC 92030601; RRID: CVCL_J052). Sex of cells is not indicated by the provider. Cell culture conditions as described above.

METHOD DETAILS

Device fabrication

Microfluidic devices were fabricated using standard photolithography and soft lithography techniques as described previously (Mazutis et al., 2013). The masters for both cell encapsulation and droplet sorting devices (see Data S2 and Data S3, and Figure S1) were fabricated on a silicon wafer (4P0/>1/525 ± 25/SSP/TTV<10, Siegert Wafer) using SU-8 3025 negative photoresist (Kayaku Advanced Materials (formerly MicroChem)) yielding a 30 μm thick layer. Following spin coating, the SU-8 was baked and patterned by UV exposure (OAI) through a high-resolution photomask (Micro Lithography Services Limited). The wafers were baked, developed, and hard-baked at 200°C for 10 min. All materials were processed according to the manufacturer's recommendations. To prevent adhesion of the PDMS during the following soft-lithography steps, the wafers were treated for 2 h with chlorotrimethylsilane (Sigma Aldrich) in a vacuum desiccator (Taccola et al., 2015). The microfluidic chips were fabricated by pouring polydimethylsiloxane (PDMS, Sylgard 184, ratio 10:1/A:B) onto the master to reach approximately 7 mm thick layer, and cured for 3 h at 70°C. The cured PDMS was carefully peeled off the master mold, and access holes were punched using a 1.02 mm hole-puncher (Syneo). The PDMS slab was then cleaned using pressurized air and scotch tape, and plasma bonded to a glass substrate (Thermo Scientific). For the droplet sorting device, metal electrodes were fabricated by filling the electrode channels with a low temperature solder (Indium Corporation) (Mazutis et al., 2013). Electrical connections were made using a short piece of wire (Alpha Wire), which was fixed to the chip using epoxy glue (Araldite). Prior to use, the microfluidic chips were treated with a filtered 5% solution of 1H,1H,2H,2H-Perfluorooctyltrichlorosilane (abcr GmbH) in isopropanol (van Swaay et al., 2015). The channels were filled with the solution and incubated for 5 min. The remaining liquid was removed using vacuum. This treatment ensured a hydrophobic PDMS surface.

Cell preparation and encapsulation

Prior to encapsulation, 7R2/A4 cells were stained with NucBlue™ Live ReadyProbes™ Reagent (Hoechst 33342) (Invitrogen) according to the manufacturer's recommendations. Stained cells were washed two times with 5 mL DPBS (Gibco). Subsequently, stained 7R2/A4 cells were mixed with unlabeled 9e10 cells at a ratio of 100:1 or 1000:1, centrifuged at 300 x g for 5 min and washed twice with 5 mL of ice-cold

DPBS. Washed cells were re-suspended in complete, ice-cold RPMI-1640 growth medium containing 16 vol % OptiPrep (Sigma-Aldrich). The assay mix contained complete, ice-cold RPMI-1640 growth medium, 16 μg/mL polyclonal goat anti-mouse (Alexa Fluor®-488) antibody (Jackson ImmunoResearch) and 8 μg/mL Alexa Fluor®-647 labeled c-myc peptide (JPT Peptide Technologies GmbH). Prior to encapsulation, the cells were concentrated to obtain 15 × 10^6 cells/mL, which according to Poisson distribution leads to a final average droplet occupancy of ~0.3 cells per 40 pl droplet.

Following preparation, the cell suspension and the assay mix were loaded into separate sterile 1 mL syringes (Omnifix), cooled with ice jackets, and injected into the microfluidic chip using PTFE tubing (0.56 × 1.07 mm, Thermo Fisher Scientific). Droplets were generated at the flow-focusing junction using 3M™ Novec™ 7500 Engineered Fluid (3M) as a carrier oil, supplemented with 1.5% (w/v) 008-FluoroSurfactant (RAN Biotechnologies). Fluids were infused into the microfluidic chip by syringe pumps (Pump 11 Pico Plus Elite, Harvard Apparatus), at flow rates of 2 μL/min for the cell suspension, 2 μL/min for the reaction solution and 6 μL/min for the continuous phase. On average, droplet generation frequency was ~2 kHz (Video S1). The cell encapsulation process was monitored using a high-speed camera (Phantom Miro M310, Vision Research) mounted onto an inverted microscope (Nikon Ti-E, Nikon). The generated droplets were collected in a 1.5 mL micro-centrifuge tube (Thermo Fisher Scientific) on ice.

Cell recovery, viability, and proliferation

To evaluate compartmentalized hybridoma viability, 9e10 cells were encapsulated in 40 pl droplets and incubated overnight for 28 h at 37°C/5% CO_2. At selected time points, a small fraction of encapsulated cells was released from the droplets by breaking the emulsion with 10% of 1H,1H,2H,2H-perfluoro-1-octanol (FluoroChem). Released cells were mixed with 0.2% (w/v) Trypan Blue solution (Gibco), incubated for 5 min at room temperature and the ratio of dead and live cells recorded using a bright field microscope and hemocytometer (Figure S2).

To evaluate proliferation capacity, 9e10 cells were encapsulated in 40 pl droplets and incubated for 3 h at 37°C/5% CO_2. Following incubation, the cells were released from droplets and transferred into pre-warmed RPMI-1640 growth media supplemented with 20% FBS, 2 mM GlutaMAX, 100 U/mL Penicillin-Streptomycin (PS), and 30% of conditioned medium (collected from 24 h 9e10 cell culture and filtered through a 0.2 μm size membrane). Cells were counted and transferred into a 96-well microtiter plate (Nunc, Thermo Fisher Scientific) by limiting dilution. Wells containing a single cell were observed over a period of 7 days.

Bulk FRET assay validation

Both desired and non-desired antibodies were harvested through centrifugation of 9e10 and 7R2/A4 hybridoma cultures respectively. Supernatant rich in antibodies was filtered through 0.2 μm size membrane and mixed with 16 μg/mL polyclonal goat anti-mouse (Alexa Fluor®-488) antibody (Jackson ImmunoResearch) and 8 μg/mL Alexa Fluor®-647 labeled c-myc peptide (JPT Peptide Technologies GmbH), resulting in the positive and negative sample mix. The control sample was prepared by mixing both detection antibody and peptide with a fresh complete RPMI-1640 cell growth medium. All samples were then analyzed on a spectrofluorometer (Horiba), using an excitation wavelength of 488 nm, recording the emission spectrum of both FRET donor and acceptor from 550 to 750 nm (Figure 1).

Antibody secretion over time

9e10 hybridoma cells were encapsulated while cooling into 40 pl droplets, along with Alexa Fluor-488 labeled polyclonal goat anti-mouse antibody, and Alexa Fluor-647 labeled c-myc peptide at 16 μg/mL and 8 μg/mL concentrations accordingly. At selected time points the FRET signal of droplets and cells was recorded under fluorescence microscope. The first time point corresponding to time 0 min was acquired immediately after finishing droplet collection off-chip on-ice (which took ~20 min). Subsequent time points were acquired at 15 min intervals during incubation at 37°C/5% CO_2. At each time-point images of the droplets were acquired using a widefield fluorescence microscope and analyzed in a semi-automated manner using a custom built MATLAB script (Figures 2 and S3A–S3D).

Antibody titration curve in droplets

A calibration curve was generated in order to determine the concentration of the secreted antibodies inside the 40 pl droplets. For this, four different reaction mixtures were generated, containing 5 to 250 nM of anti-c-myc antibody (Millipore). These reaction mixtures were then encapsulated into 40 pl droplets, together with 16 μg/mL polyclonal goat anti-mouse (Alexa Fluor®-488) antibody (Jackson ImmunoResearch) and 8 μg/mL Alexa Fluor®-647 labeled c-myc peptide (JPT Peptide Technologies GmbH). After a 30 min incubation at 37°C/5% CO_2, the emulsions were transferred into hybridization chambers (Grace Bio-Labs) mounted on a coverslip, and images of each sample were acquired on an inverted microscope (Nikon), equipped with a bright field lamp (CoolLED), fluorescence light source (Omicron) and sCMOS camera (Photometrics).

Digital Images of recorded droplets were analyzed using a custom-built MATLAB script (Figures S3A–S3D and Data S1), which identifies droplets in the bright-field channel using a circular Hugh transformation (CHT) followed by binarization. The generated binary mask is then applied to the original fluorescence image, and the sum fluorescence intensity of each droplet is calculated as the sum of all pixel values. Background correction is applied by subtracting the sum fluorescence intensity of droplets not containing any desired Ab from the droplets at each assessed Ab concentration value.

Quantitative droplet image analysis

Images of droplets were analyzed using a custom-built MATLAB script (Figures S3A–S3D and Data S1). Images were initially loaded from hyperstacks and divided into individual color channels, i.e. brightfield (BF) and FRET acceptor fluorescence (FL). To compensate for uneven focus throughout the field of view (FOV) images were divided into several regions, with each region focused individually. Droplets were initially identified in the brightfield channel through Circle Hough Trans-form (CHT) and subsequently separated into droplets containing a single cell (Figures S3A and S3B, blue outline) and droplets containing no or multiple cells (Figure S3A, red outline). CHT specifically identifies round objects within a specified radius range, therefore only droplets of a desired size were analyzed, with droplets partially reaching out of the field of view (FOV) excluded from the analysis. Each droplet was cropped from the original image and a binary mask was generated and applied, separating the inside from the outside of the droplet for further analysis. Cells within droplets were initially identified using a second round of CHT (Figure S3A and C, green outline). Individual cell images were cropped following this rough identification and cells precisely identified using the Canny edge detection method. The binary mask generated by edge detection followed by dilation and erosion was then applied to the raw images separating the cell from its surroundings. Parameters for edge detection as well as dilation and erosion of the mask were chosen manually such that all cells could be identified as closely as possible. Cell fluorescence intensity was quantified as sum of all nonzero pixels in the masked image, and likewise the cell area was quantified as the number of nonzero pixels in the masked image. Droplet fluorescence was quantified in the same manner, with the fluorescence intensity integral equal to the sum of all nonzero pixels, and the droplet area equal to the number of all nonzero pixels in the masked droplet image. Fluorescence emanating from the cells was subtracted from the droplet fluorescence intensity integral for all following analysis steps. Background fluorescence was quantified in all droplets containing no cells, following the same approach as described above and subtracted from the quantified fluorescence intensity values.

FRET-activated droplet sorting

Droplets prepared as described above were incubated off-chip for 30 min at 37°C/5% CO_2 and re-injected into a second microfluidic device designed for FRET-activated droplet sorting (Figure S1B and Data S3). The sorting device consisted of a droplet re-injection inlet, two auxiliary oil inlets and a Y-shaped junction from which the collection and waste channel branch off. The additional oil was used to space and transport the densely packed droplets coming from the re-injection inlet. This is crucial, as droplets have to be well separated from one another so that they can be sorted efficiently. Once re-injected, the droplets are carried along a narrow channel, eventually passing through a laser beam aligned to the microfluidic device. Downstream of this interrogation point the microfluidic channel is divided in two separate channels: one used to collect droplets of interest and the other leading to waste. The hydrodynamic pressure between these two channels is carefully tuned such that without any external influence all droplets are carried to the waste channel. Along the channel, right at the intersection of the collection and waste channel, three electrodes are positioned. Through these electrodes, a positive dielectrophoretic force is applied on a single passing droplet, efficiently sorting droplets of interest from a stream of droplets (see Video S2).

All sorting experiments were carried out on an inverted microscope equipped with a 488 nm diode laser (Omicron-laserage Laserprodukte GmbH) and two photomultiplier tubes (PMTs) (Hamamatsu) for fluorescence detection (Figures S3E and S3F). The laser beam was expanded and shaped into a line using a cylindrical lens (Thorlabs) and projected onto the microfluidic device using a 20X objective (Nikon). Fluorescence signals were recorded and processed online using a field-programmable gate array (FPGA) (National Instruments) and custom LabVIEW program (National Instruments). Both donor and acceptor fluorescence were recorded simultaneously using both PMTs. In case the detected intensity exceeded a predefined threshold, a square wave pulse was sent from the FPGA card to a high voltage amplifier (Trek Inc.), and from the amplifier to the electrodes embedded within the chip, resulting in the displacement of a single droplet to the collection channel. Sorting experiments were generally carried out at frequencies of approximately 500 Hz.

Post-sorting image acquisition

Static images were acquired by injecting a small amount of the emulsion into hybridization chambers (Grace Bio-Labs) mounted on a coverslip. Three samples were imaged: droplet emulsion right before sorting, sorted droplets, and droplets collected from the waste channel. After loading the samples, the imaging chambers were mounted on an inverted microscope equipped with a fluorescence lamp (Lumencor Inc.) and camera (PCO AG), and imaged using a 20X objective (Nikon). Fluorescence images of the FRET-signal and the Hoechst 33342 stain were acquired to verify the sorting results by quantifying the number of positive hits, false positive events and non-sorted droplets, as well as cells contained within. Images were analyzed using a custom MATLAB script used to automatically count the number of droplets found in each image. The results were validated manually, and the number of cells, as well as the fluorescence signals, quantified (Figure S5 and 3B).

Antibody quantification by ELISA

Cell supernatants were analyzed to determine antibody fraction before and after droplet sorting-based enrichment. First, sorted droplets (n = 624 droplets) were chemically broken to release encapsulated cells, which were collected and transferred into a 24-well cell culture plate (Thermo Scientific) containing 1 mL of pre-warmed RPMI-1640 medium supplemented with 20% FBS, 2 mM GlutaMAX and 100 U/mL PS. The same number of cells from the pre-sorting sample was seeded in another well. Cells in both wells were cultured for 12 days, after which the supernatants from the expanded cell cultures were collected, filtered through a 0.2 μm size membrane, and analyzed by a standard enzyme-linked immunosorbent assay (ELISA). For ELISA, 96-well half-area, flat bottom plate (Corning) was coated with two different antigens: the first half of the plate was coated with 100 ng/mL and 200 ng/mL of IFN-gamma (Sigma Aldrich), and the other half – with 100 ng/mL and 200 ng/mL c-myc peptide (Sigma Aldrich). Both antigens were suspended in carbonate-bicarbonate buffer (Sigma Aldrich) and distributed at 30 μL/well. Coated plates were incubated while shaking at 4°C, overnight. After coating, wells were washed three times with 200 μL/well of the wash buffer (1X PBS with 0.05% Tween 20) and incubated for 1 h with blocking solution (5% non-fat dry milk, Sigma Aldrich), while shaking at room temperature. After blocking, wells were washed three times with 200 μL/well of the wash buffer before 50 μL of the supernatants from the sorted and non-sorted cell cultures were loaded into wells coated with both antigens. Following incubation and three rounds of washing, 30 μL/well Goat polyclonal anti-mouse (HRP) secondary antibody (1:4000 diluted in 0.5% milk/PBS, Biolegend) were added and incubated while shaking for 45 min, at room temperature. After this step, the washing procedure was repeated three times and 30 μL/well of TMB (Sigma Aldrich) substrate was added and incubated until the color of the solution has changed to the expected color. The reaction was then stopped by adding 15 μL/well of 1M H_2SO_4 (Panreac AppliChem). Finally, the absorbance was measured at 450 nm (Tecan) (Figure 5).

QUANTIFICATION AND STATISTICAL ANALYSIS

Results are presented as either absolute values or mean +/− standard deviation, with the sample number n stated wherever relevant.

ADDITIONAL RESOURCES

Does not apply.